

Thiazoloisoindigo-based Ambipolar Polymer for Excellent Balanced Hole and Electron Mobility

Author Bowen Li^{a*}, Xiangyu Zou^a, Qiyi Li^b, Kang Xu,^d Youbing Mu^{a*}, Jieyu Wang^b, Jian Pei^b,
Chunming Yang^c, Zhenggang Lan,^d Xiaobo Wan^{a*}

^aSchool of Chemical & Environmental Engineering, Key Laboratory of Optoelectronic Chemical Materials and Devices, Ministry of Education, Jiangnan University, Wuhan, P. R. China

^bBeijing National Laboratory for Molecular Sciences, the Key Laboratory of Bioorganic Chemistry and Molecular Engineering of Ministry of Education, College of Chemistry and Molecular Engineering, Peking University, Beijing 100871, P. R. China

^cShanghai Synchrotron Radiation Facility, Shanghai Advanced Research Institute, Chinese Academy of Sciences, Shanghai, 201204, P. R. China

^dSCNU Environmental Research Institute, Guangdong Provincial Key Laboratory of Chemical Pollution and Environmental Safety & MOE Key Laboratory of Environmental Theoretical Chemistry, School of Environment, South China Normal University, Guangzhou 510006, P. R. China

Contents

1. Synthesis
2. Quantum Chemical Calculations
3. High temperature GPC analysis
4. Thermogravimetric Analysis
5. Electrochemical Characterization
6. Photophysical Characterization
7. OFET Fabrication and Characterization
8. X-ray diffraction and morphology Study

1. Synthesis

1.1. Synthesized of polymers P(T-TzII-T-DPP)-C12, P(T-TzII-T-DPP)-C20, P(Se-TzII-T-DPP)-C12, and P(Se-TzII-T-DPP)-C20.

All reagents and solvents used for the synthesis of the compound were purchased from commercial source and used without further purification. TzII-T-Br are synthesized according our previous work¹.

Synthesized of polymers P(T-TzII-T-DPP)-C12. Th-TzII-Br (119.4 mg, 0.08 mmol), stannyl-Th-BT-H (50.08 mg, 0.08 mmol), Pd₂(dba)₃ (1.47 mg) and P(*o*-tol)₃ (3.90 mg) and 5 mL of toluene were added to a Schlenk tube. The tube was charge with Ar through a freeze-pump-thaw cycle for three times. The mixture was stirred for 72 h at 110 °C. And then the mixture was precipitated into methanol (100 mL). The precipitate was filtered and purified via Soxhlet extraction for 8 hours with methanol, 12 hours with hexane, 12 hours with chloroform, and finally was collected with *o*-DCB. The chloroform solution was then concentrated and precipitated into methanol (100 mL) to give a dark-green solid (127.4 mg, 97.2%).

Synthesized of polymers P(T-TzII-T-DPP)-C20. Th-TzII-Br (119.4 mg, 0.08 mmol), stannyl-T-DPP-C20 (63.7 mg, 0.08 mmol), Pd₂(dba)₃ (1.47 mg) and P(*o*-tol)₃ (3.90 mg) and 5 mL of toluene were added to a Schlenk tube. The tube was charge with Ar through a freeze-pump-thaw cycle for three times. The mixture was stirred for 72 h at 110 °C. And then the mixture was precipitated into methanol (100 mL). The precipitate was filtered and purified via Soxhlet extraction for 8 hours with methanol, 12 hours with hexane, 12 hours with chloroform, and finally was collected with *o*-DCB. The chloroform solution was then concentrated and precipitated into methanol (100 mL) to give a dark-green solid (142.3 mg, 98.7%).

Synthesized of polymers P(Se-TzII-T-DPP)-C12. Th-TzII-Br (119.4 mg, 0.08 mmol),

stannyl-T-DPP-C12 (50.08 mg, 0.08 mmol), Pd₂(dba)₃ (1.47 mg) and P(*o*-tol)₃ (3.90 mg) and 5 mL of toluene were added to a Schlenk tube. The tube was charge with Ar through a freeze-pump-thaw cycle for three times. The mixture was stirred for 72 h at 110 °C. And then the mixture was precipitated into methanol (100 mL). The precipitate was filtered and purified via Soxhlet extraction for 8 hours with methanol, 12 hours with hexane, 12 hours with chloroform, and finally was collected with *o*-DCB. The chloroform solution was then concentrated and precipitated into methanol (100 mL) to give a dark-green solid (127.4 mg, 97.2%).

Synthesized of polymers P(Se-TzII-T-DPP)-C20. Th-TzII-Br (119.4 mg, 0.08 mmol), stannyl-T-DPP-C20 (63.7 mg, 0.08 mmol), Pd₂(dba)₃ (1.47 mg) and P(*o*-tol)₃ (3.90 mg) and 5 mL of toluene were added to a Schlenk tube. The tube was charge with Ar through a freeze-pump-thaw cycle for three times. The mixture was stirred for 72 h at 110 °C. And then the mixture was precipitated into methanol (100 mL). The precipitate was filtered and purified via Soxhlet extraction for 8 hours with methanol, 12 hours with hexane, 12 hours with chloroform, and finally was collected with *o*-DCB. The chloroform solution was then concentrated and precipitated into methanol (100 mL) to give a dark-green solid (142.3 mg, 98.7%).

2. Quantum Chemical Calculations

All of the theoretical simulations for the investigated molecules were performed using the Gaussian 09 program package. The electron density distribution of frontier molecular orbital (FOM) was visualized with Gaussview 3.0. Structure optimizations were carried out using density functional theory (DFT) calculations. The ground state structures were optimized with B3LYP/6-31G (p,d) level set in the gas phase according to the reference[1]. In addition, the electron density (ρ) and Laplacian of electron density ($\nabla^2\rho$) for intramolecular noncovalent interactions are calculated and conducted using Multifwn. [2]

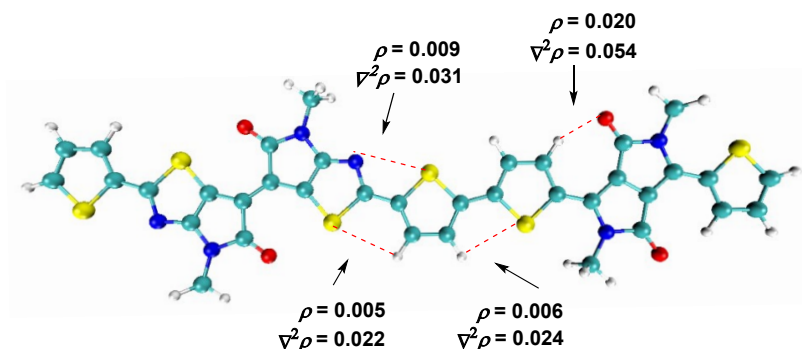


Figure S1. The electron density (ρ) and Laplacian of electron density ($\nabla^2\rho$) for N \cdots S, S-H, and S-O.

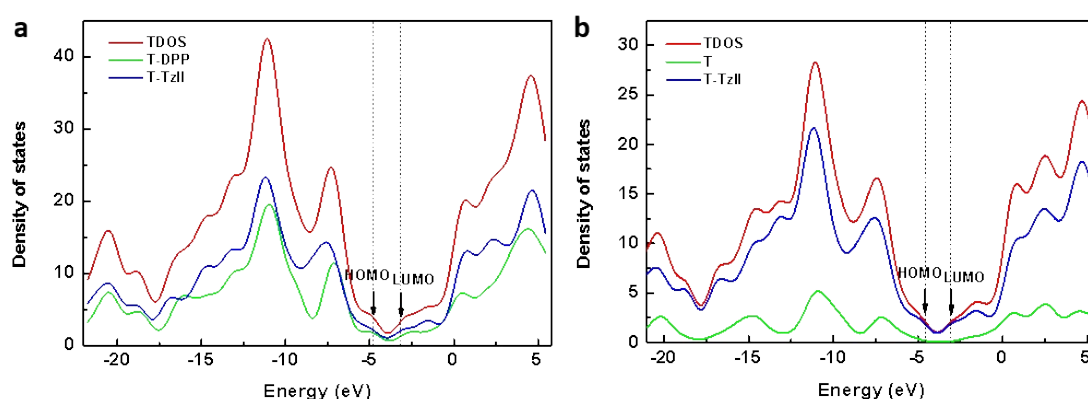


Figure S2. The partial density of states (DOS) of (a) the monomer (T-TzII-T-DPP) of polymer P(T-TzII-DPP-T)-C12/C20 and (b) the monomer (TzII-T-T-T) of polymer P1, where alkyl chains are replaced by methyl.

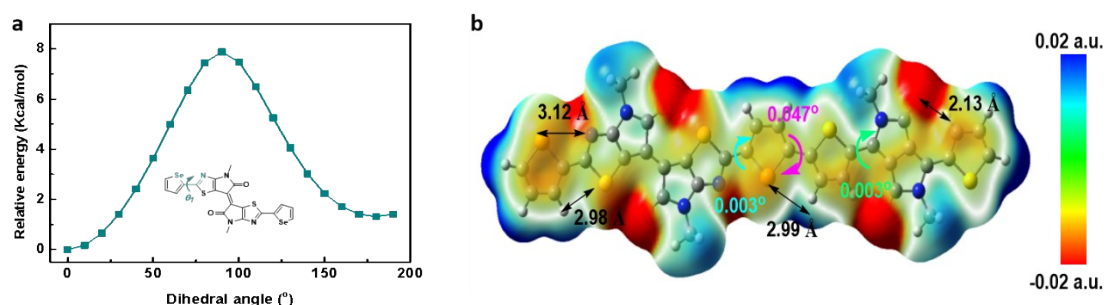


Figure S3. (a) Dihedral potential energy scans as a function of the dihedral angles between TzII and selenophene (θ_1) units of Se-TzII-T-DPP monomer. (c) Optimized ground state configuration, electrostatic potential map (isovalue: 0.02 a.u.). Geometries were optimized using B3LPY/6-31G(d,p) levels, and all alkyl chains are substituted with methyl unit for simplicity.

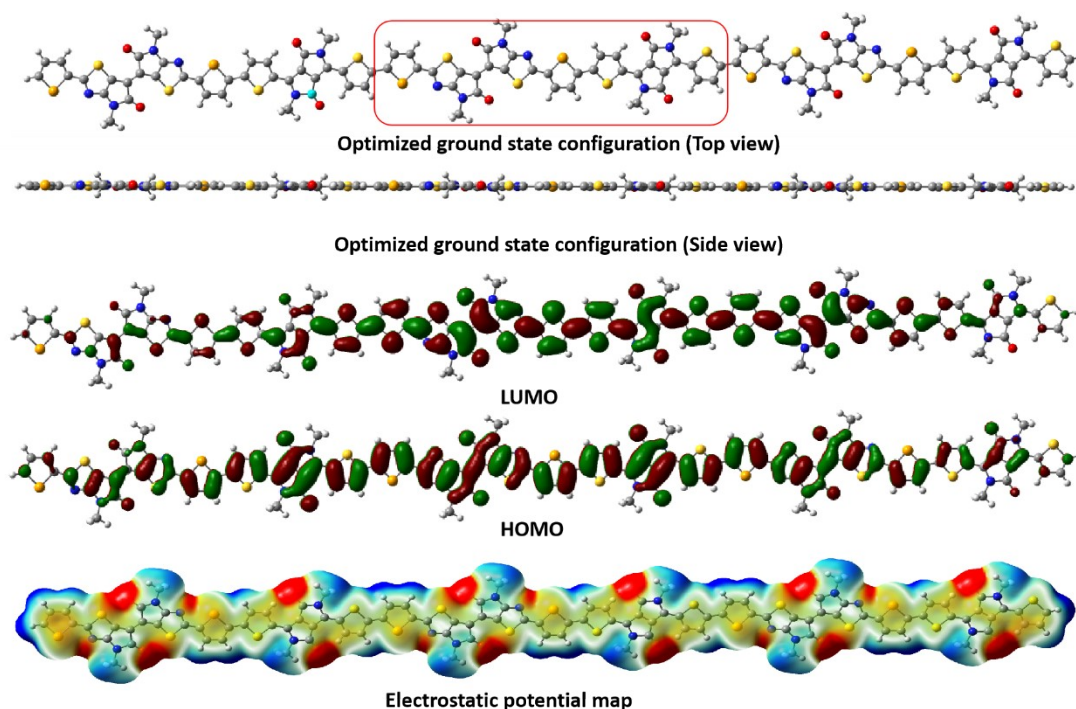


Figure S4. Optimized trimer ground state configuration, HOMO and LUMO orbital distribution, and electrostatic potential map (isovalue: 0.02 a.u.) of Se-TzII-T-DPP. Geometries were optimized using B3LPY/6-31G(d,p) levels, and all alkyl chains are substituted with methyl unit for simplicity.

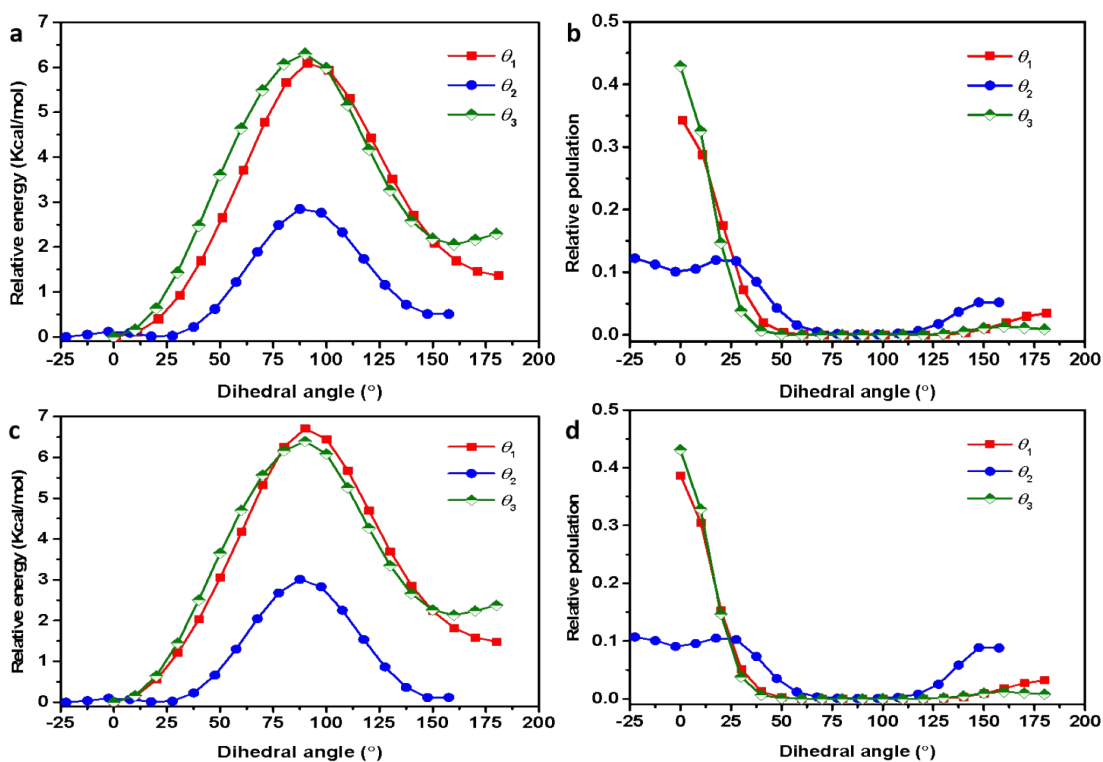


Figure S5 Dihedral potential energy scans and conformation distribution as a function

of the dihedral angles between **TzII** and thiophene or selenophene (θ_1) units, thiophene and thiophene (θ_2) units, thiophene and **DPP** (θ_3) units in (a,b) **T-TzII-T-DPP** monomer and (c,d) **Se-TzII-T-DPP** monomer using ω B97xd as the calculation level.

3. High temperature GPC analysis

The molecular weights of the polymers were measured by the gel permeation chromatography (GPC) performed on Waters 1151 pump and UV-vis monitor (700 nm) using 1,2,4-trichlorobenzene (TCB) as eluent (150 °C).

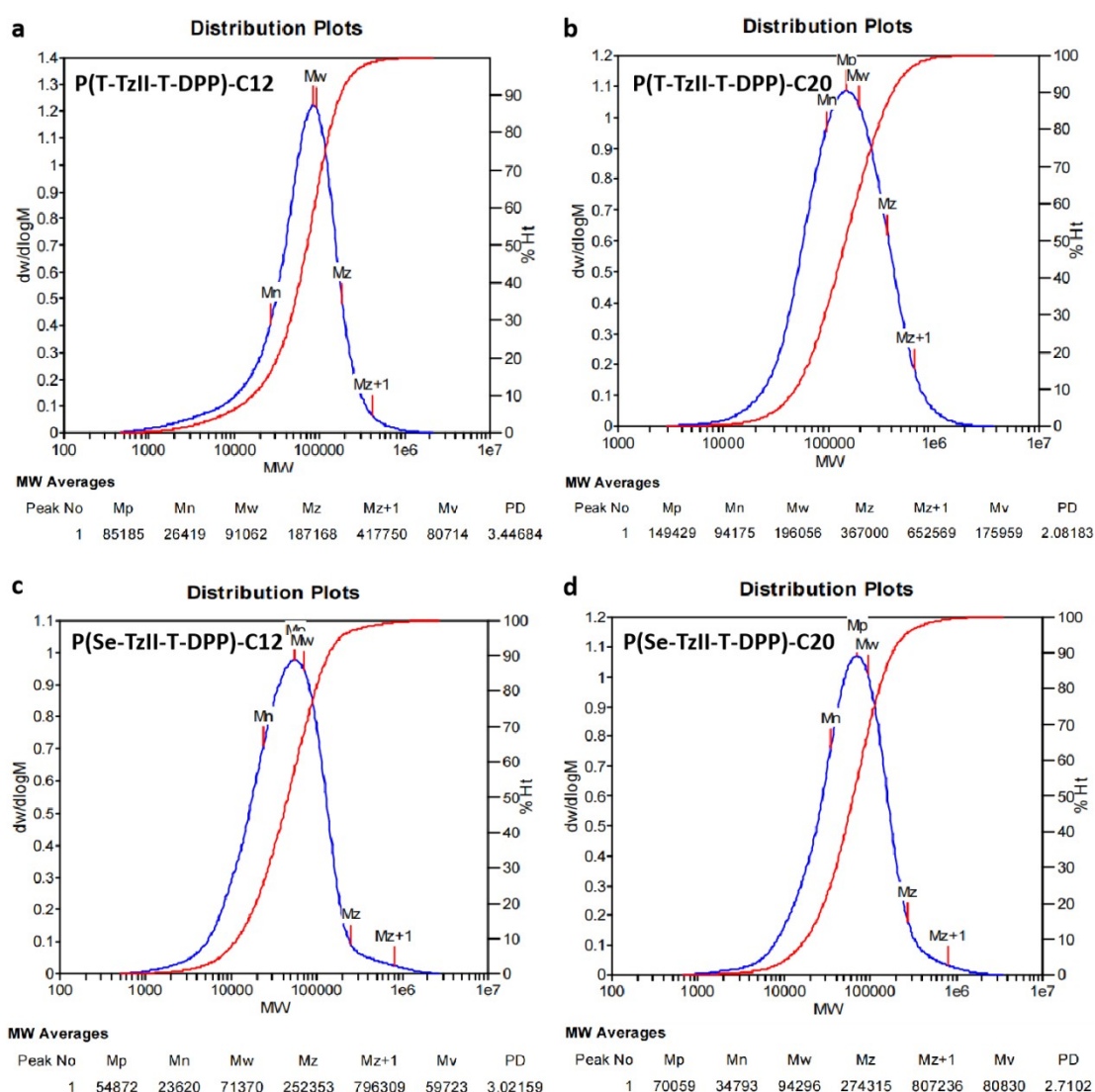
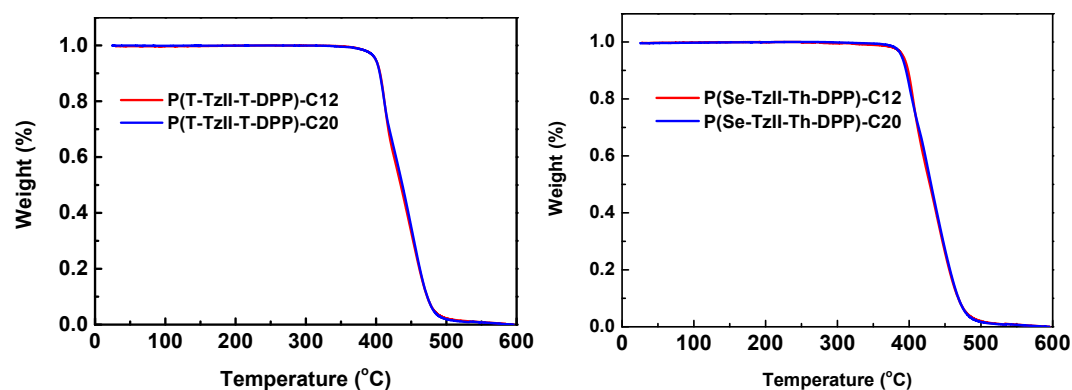


Figure S6. GPC of P(T-TzII-T-DPP)-C12, P(T-TzII-T-DPP)-C20, P(Se-TzII-T-DPP)-C12, and P(Se-TzII-T-DPP)-C20.

4. Thermogravimetric Analysis

The thermal properties of P(T-TzII-T-DPP)-C12, P(T-TzII-T-DPP)-C20, P(Se-TzII-T-DPP)-C12, and P(Se-TzII-T-DPP)-C20 were investigated by thermogravimetric analysis (TGA). Thermal gravity analyses (TGA) were carried out on a NETZSCH STA 449F5 analyzer. Sample preparation: weigh 5-6 mg samples and cut them into smaller pieces or other shapes for later use. Weigh the quality of the Al crucible with a balance, remove the Al crucible weight (zero) and take it out. Then put the sample into the Al crucible, weigh it again, and record the quality of the sample. Put it on the tray of sampler, then take out the Al crucible data cover with tweezers, cover the Al crucible on the cochlear, put it into the DSC sampler sample preparation, sample pressing 2 times. Pick up the furnace cover of DSC sample pool with tweezers, put the prepared sample into the annular area of the left sample pool with tweezers (small point at the bottom of the aluminum pot) and jam, and cover the furnace well with tweezers. Thermogravimetric analysis (TGA) was undertaken with a METTLER TOLEDO TGA2 instrument. Differential scanning calorimetry (DSC) was performed on a NETZSCH DSC 200 PC unit at a heating rate of 10°C min⁻¹ from 0 to 300°C under nitrogen atmosphere. The second heating scan were recorded, as shown in Figure S7.



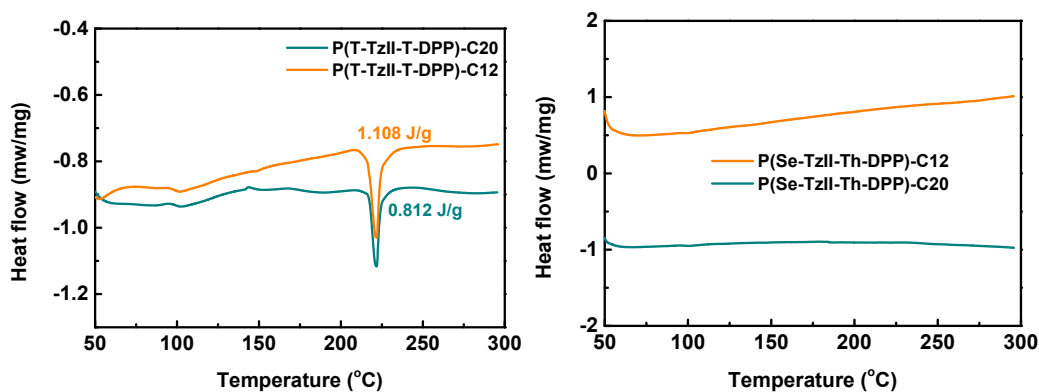


Figure S7. TGA curves and DSC curves of P(T-TzII-T-DPP)-C12, P(T-TzII-T-DPP)-C20, P(Se-TzII-T-DPP)-C12, and P(Se-TzII-T-DPP)-C20.

5. Electrochemical Characterization

The oxidation potential was determined by cyclic voltammetry using 0.1 M tetrabutylammonium hexafluorophosphate (TBAPF₆) in CH₃CN as a supporting electrolyte and a scan rate of 50-100 mV s⁻¹. glassy carbon electrode, Ag/AgCl and Pt mesh were used as working electrode, reference electrode and counter electrode, respectively. A three-electrode cell comprising silver/silver chloride (Ag/AgCl), a platinum mesh and ITO as the reference, counter, and working electrodes, respectively, were used. The highest occupied molecular orbit (HOMO) energy levels were determined by calculating the empirical formula of $E_{\text{HOMO}} = -e(E_{\text{ox}} + 4.8 - E_{1/2}^{\text{(Fc/Fc+)}})$ where E_{ox} was the onset oxidation potential. The lowest unoccupied molecule orbital (LUMO) energy levels were determined by calculating the empirical formula of $E_{\text{LUMO}} = -e(E_{\text{re}} + 4.8 - E_{1/2}^{\text{(Fc/Fc+)}})$, where E_{re} was the onset reduction potential.

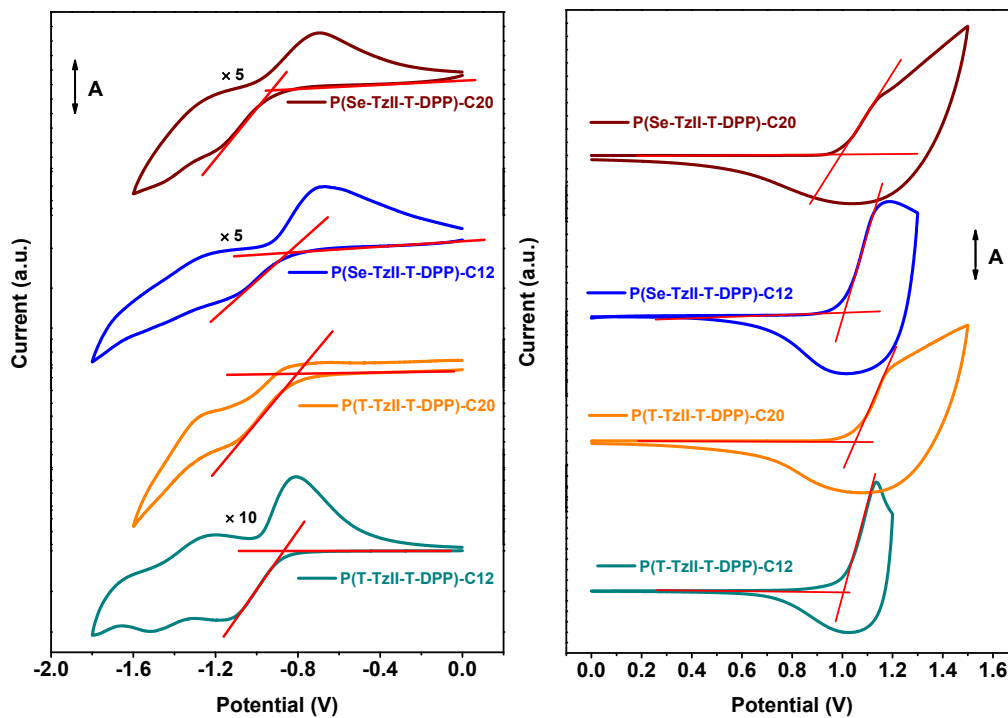
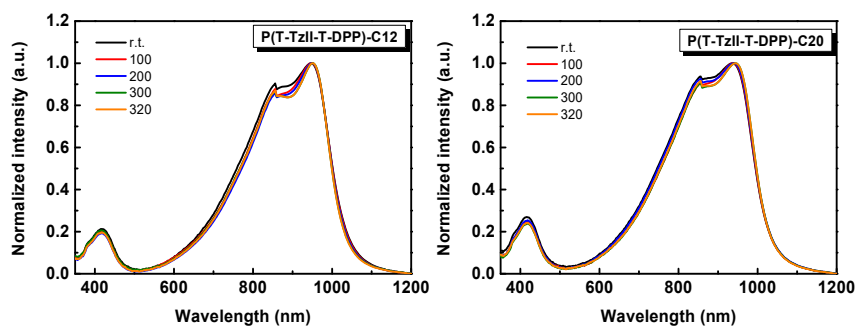


Figure S8. Cyclic voltammogram of P(T-TzII-T-DPP)-C12, P(T-TzII-T-DPP)-C20, P(Se-TzII-T-DPP)-C12, and P(Se-TzII-T-DPP)-C20.

6. Photophysical Characterization

The UV-Vis spectra were collected with a Hitachi U-4100 UV-vis spectrophotometer in an anhydrous *o*-dichlorobenzene solution (1×10^{-5} g L⁻¹) or on a quartz glass by coating polymer solution (5 mg/mL).



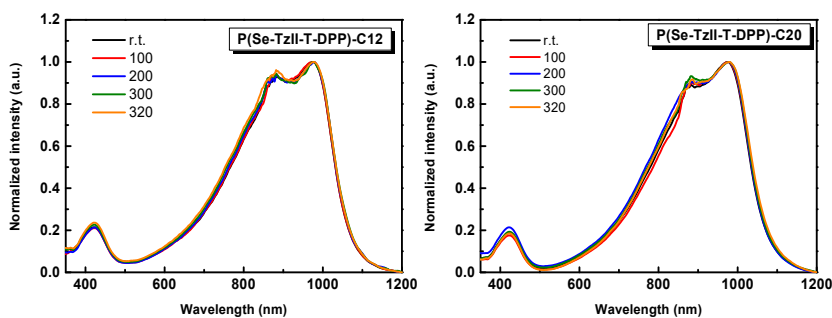


Figure S9 UV-vis spectra of four polymers

7. OFET Fabrication and Characterization

OFET fabrication: Four polymers P(T-TzII-T-DPP)-C12, P(T-TzII-T-DPP)-C20, P(Se-TzII-T-DPP)-C12 and P(Se-TzII-T-DPP)-C20 was dissolved at 100 °C overnight and then the solution (5 mg/mL) was purified by a filter of 0.45 μm aperture. Si/SiO₂ patterned with Au substrate were firstly sequentially cleaned with acetone, deionized water (three times) and isopropyl alcohol using ultrasonication and then dried under vacuum at 100 °C for 10 min. The polymer solution was warmed to 100 °C for 10 min, and then was heated to 120 °C for 5 min. The semiconducting layer was deposited onto the patterned Si/SiO₂/Au substrates by spin-coating while the polymer solution is hot (2000 r/s for 1 min, and then 3000 r/s for 3 s), followed by thermal annealing at 280 °C for 10 min. A CYTOP solution was spin-coated as the dielectric layer (2000 r/s for 1 min, and then 3000 r/s for 3 s). After thermal annealing at 100 °C for 1 h, an aluminum layer was thermally evaporated as the gate electrode under high vacuum up to 4×10^{-5} Pa (450 Å, the rotate speed less than 2 Å/s).

OFET characterization: The electrical characterization of the OFETs was carried out using a Keithley 4200 SCS semiconductor parameter analyzer. The field-effect mobility (μ) was calculated from the saturation transfer characteristics according to the following equation:

$$I_{SD} = W/2L C_i \mu (V_G - V_T)^2$$

where I_{SD} is drain current, W and L are the channel width and length, respectively. C_i (3.7 nF cm⁻² for CYTOP) is the capacitance per unit area. V_G and V_T are the applied gate bias and threshold voltage, respectively. In this work, the W/L of all OFET devices are 20, but W and L is variable (L = 5, 10, 20, 50, and 100 μm , corresponding to W =

100, 200, 400, 1000, and 2000, respectively).

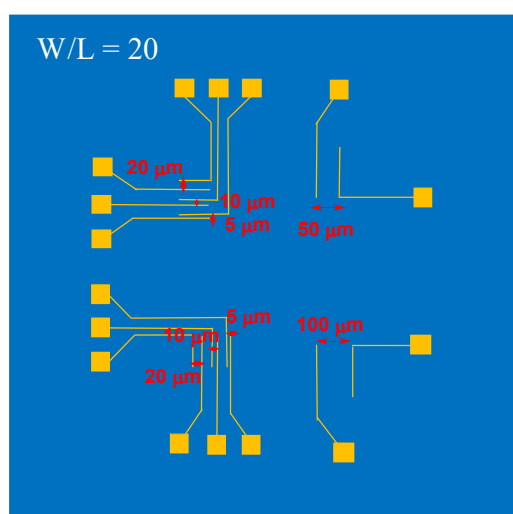


Figure S10. The OFET devices used in this work to optimize W, L, and annealing temperature. Notably, the W/Ls of all OFET devices are 20.

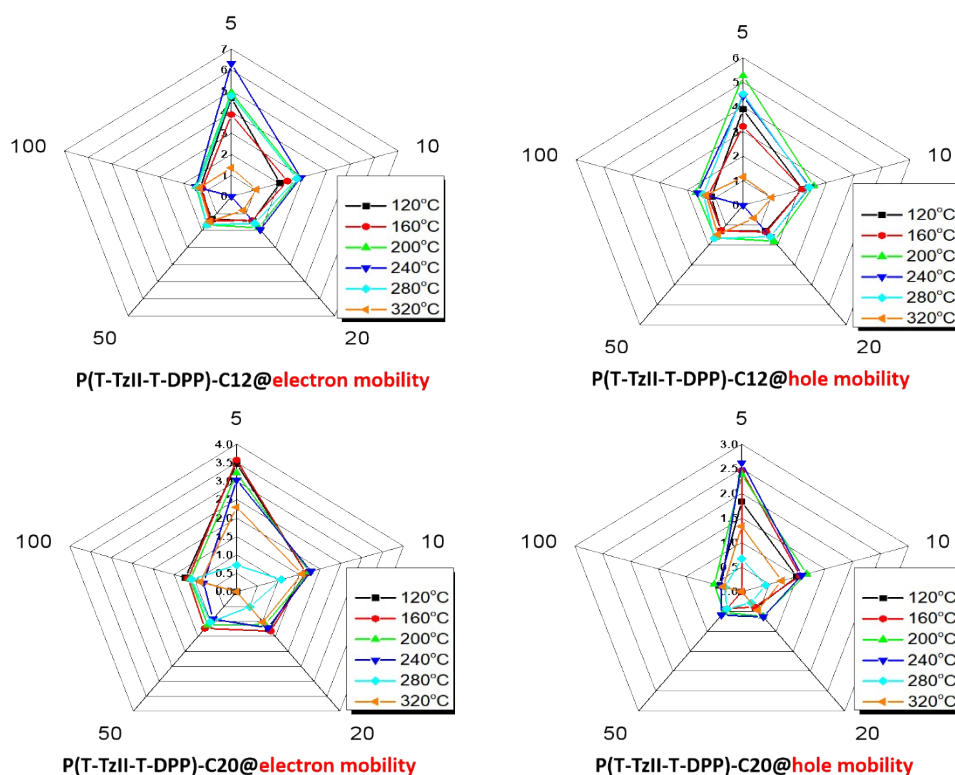


Figure S11. Maximum carries mobilities of P(T-TzII-T-DPP)-C12 and P(T-TzII-T-DPP)-C20 annealing at different temperature. The OFET devices has the same ratio of channel width and length ($W/L = 20$), but has different L (5, 10, 20, 50, and 100 μm).

Table S1. The average carries mobilities (8 devices) of P(T-TzII-T-DPP)-C12, P(T-TzII-T-DPP)-C20, P(Se-TzII-T-DPP)-C12, and P(Se-TzII-T-DPP)-C20 annealing at

different temperatures.

Polymers	Tem. (°C)	μ_e^a (cm ² V ⁻¹ s ⁻¹)	μ_h^a (cm ² V ⁻¹ s ⁻¹)	μ_e/μ_h^a
P(T-TzII-T-DPP)-C12	120	1.87	1.76	1.06
	160	1.53	1.81	0.85
	200	2.21	2.57	0.86
	240	2.65	2.47	1.07
	280	3.43	2.81	1.22
	320	1.53	1.70	0.90
P(T-TzII-T-DPP)-C20	120	1.59	1.18	1.35
	160	1.63	0.96	1.70
	200	1.71	1.46	1.17
	240	1.48	0.91	1.62
	280	1.61	1.28	1.26
	320	1.41	0.69	2.04
P(Se-TzII-T-DPP)-C12	120	0.37	0.74	0.50
	160	0.36	0.49	0.73
	200	0.29	0.42	0.69
	240	0.06	0.26	0.23
	280	1.70	2.13	0.80
	320	0.08	0.27	0.30
P(Se-TzII-T-DPP)-C20	120	0.74	0.44	1.68
	160	0.61	0.37	1.65
	200	0.26	0.34	0.76
	240	0.24	0.23	1.04
	280	0.62	0.48	1.29
	320	0.22	0.19	1.16

^aThe OFET devices has the same ratio of channel width and length (W/L = 20), but has different L (5, 10, 20, 50, and 100 μm).

Table S2. Summarized OFET device performances of P(T-TzII-T-DPP)-C12 annealing at different temperatures.

P(T-TzII-T-DPP)-C12@Temperature (°C) ^a						
	120	160	200	240	280	320
1	4.6646/3.9002	3.8783/3.2148	4.9324/5.2734	6.2962/4.4272	5.6993/4.5249	2.8300/3.2693
2	1.9508/2.0832	-/1.9389	4.6095/9.0653	4.6113/5.2784	6.5924/6.1080	2.5097/1.4391
3	1.5417/1.3997	1.4084 /1.3467	2.5732/2.8255	2.3906/2.4354	2.7634/2.8235	1.2473/2.4656
4	1.2091/1.1432	0.9859/0.9243	2.8188/2.5418	2.9094/2.4040	3.2787/2.6947	1.5522/1.1090

5	3.5698/3.0074	1.4327 /	1.8370/1.8091	1.9569/1.5792	1.9733/1.7479	0.9612/1.6632
6	2.0335/2.1250	3.4654/3.7387	1.6215/1.8659	1.7453/1.6701	1.9732/1.9636	1.3918/0.6090
7	1.4386/1.3012	2.3546/2.1266	1.6616/1.6193	1.4921/1.6300	2.0982/1.7169	0.9771/1.3879
8	1.3255/1.2753	1.3262/1.4795	1.4833/1.6818	2.9345/2.8405	5.7853/4.6267	0.8815/1.4135
9	1.1292/1.0759	1.4166/1.2738	0.7728/2.9568	3.1374/2.7527	2.9045/1.2346	0.8003/1.8213
10			0.1534/0.7441	1.3843/1.6107	2.9322/2.3605	0.2416/1.0665
11			0.5812/0.6960		1.5348/0.8311	0.4514/1.1407
12			0.2993/0.4367		1.8674/1.4555	0.5223/0.7431
13			0.2920/0.6114		0.7880/0.6509	1.7663/0.5960
14			1.0647/0.4350		0.6449 /0.7827	1.9386/1.8503
15			0.2904/0.3922			
Ave	1.87/1.76	1.53/1.81	2.21/2.57	2.65/2.47	3.43/2.81	1.53/1.70
.						
Dev	0.81/0.68	0.41/0.71	1.13/1.21	1.00/0.94	1.49/0.98	0.52/0.41
.						

^aThe OFET devices has the same ratio of channel width and length ($W/L = 20$), but has different L (5, 10, 20, 50, and 100 μm). Electron (μ_e) and hole (μ_h) mobility were expressed as μ_e/μ_h , respectively, in Table. The bold fonts of μ_e/μ_h were used to calculate the average μ_e/μ_h . Dev. is the deviations.

Table S3. Summarized OFET device performances of P(T-TzII-T-DPP)-C20 annealing at different temperatures.

P(T-TzII-T-DPP)-C20@Temperature ($^{\circ}\text{C}$) ^a						
	120	160	200	240	280	320
1	3.4693/1.8270	3.5747/2.4646	2.9488/3.1317	3.0358/2.6159	2.0931/1.6560	1.9717/1.0028
2	0.7021/1.2800	1.0029/0.7016	3.2124/2.3789	1.1382/0.6603	1.3024/1.4942	1.9956/1.2239
3	1.6605/0.9917	1.6638/1.0520	1.7409/1.1699	0.9249/0.5885	1.4697/0.8392	0.9025/0.4453
4	1.2451/0.4092	1.3211/0.3832	1.5368/1.1508	0.7872/0.3748	0.8688/0.4921	1.1956/0.5108
5	1.2347/0.4148	0.8060/0.4271	0.7078/0.6733	3.0376/2.1572	0.8831/0.5756	0.8313/0.3542
6	2.7520/2.2116	1.2332/0.4521	1.1047/0.6237	1.7784/1.0802	2.7236/2.6466	0.8586/0.4220

7	1.6702/0.8727	1.1552/-	0.8763/0.5068	1.2139/0.6272	2.6882/2.8625	1.9915/1.5309
8	0.9632/0.5379		1.1135/0.4936		1.4846/-	1.9798/0.9834
9			2.4237/3.0317		1.6935/ -	1.2028/0.5358
10			1.6814/1.1771		1.0538/ -	1.1970/0.4704
11			1.0274/0.6544		1.1196/ -	0.8678/0.3636
12			1.1156/0.5185		0.8025/-	0.7793/0.3035
13			0.8776/0.3891			0.7166/0.2701
Ave.	1.59/1.18	1.63/0.96	1.71/1.46	1.48/0.91	1.61/1.28	1.41/0.69
Dev.	0.63/0.64	0.99/0.89	0.67/0.86	0.84/0.91	0.55/0.82	0.49/0.33

^aThe OFET devices has the same channel width and length ($W/L = 20$), but has different W (5, 10, 20, 50, and 100 μm). Electron (μ_e) and hole (μ_h) mobility were expressed as μ_e/μ_h , respectively, in Table. The bold fonts of μ_e/μ_h were used to calculate the average μ_e/μ_h . Dev. is the deviations.

Table S4. OFET parameters for four polymers **P(T-TzII-T-DPP)-C12**, **P(T-TzII-T-DPP)-C20**, **P(Se-TzII-T-DPP)-C12** and **P(Se-TzII-T-DPP)-C20** films annealed at 280 °C.

	P(T-TzII-T-DPP)	P(T-TzII-T-DPP)	P(Se-TzII-T-DPP)	P(Se-TzII-T-DPP)
	-C12	-C20	-C12	-C20
1	4.0211/5.1871	3.2315/1.4896	1.3174/1.8411	0.5657/0.5291
2	5.4771/5.4871	3.0114/2.6065	1.3668/2.0060	0.7245/0.3717
3	7.3298/5.7117	2.2589/1.0594	2.0004/2.3819	0.5780/0.4396
4	5.7673/5.7998	3.3808/2.1176	1.8401/2.5539	0.6472/0.3768
5	7.2095/5.0404	3.8311/1.8560	2.0892/1.9496	0.5837/0.5068
6	5.4895/6.1946	3.5662/2.1856	1.0956/2.1409	0.5341/0.3877
7	7.6214/6.3127	2.2676/0.7086	0.8674/1.7387	0.5576/0.4383
8	3.8632/2.6809	2.5692/2.4179	0.7966/1.7521	0.6625/0.4428
9	5.9267/5.6738	2.9511/1.3823	1.7883/2.1888	0.5995/0.6268
10	-/6.0077	2.7878/1.8077	1.9934/2.2548	0.6747/0.4713

11	6.2496/5.9975	3.1617/2.0024	1.6787/2.1568	0.5737/0.4890
12	5.6993/4.5249	2.9577/2.0696	1.4636/2.1108	0.6040/0.5429
13	6.5924/6.1080	3.2018/1.8706	2.1133/1.8950	0.6439/0.4396
14		2.0931/1.6560		
15		2.7236/2.6466		
16		2.6882/2.8625		
Ave.	6.29/5.77	3.08/2.16	1.70/2.13	0.62/0.48
Dev.	0.75/0.41	0.36/0.32	0.35/0.21	0.05/0.07

The OFET devices has the same channel width and length ($L=5\ \mu\text{m}$, and $W=100\ \mu\text{m}$). Electron (μ_e) and hole (μ_h) mobility were expressed as μ_e/μ_h , respectively, in Table. The bold fonts of μ_e/μ_h were used to calculate the average μ_e/μ_h . Dev. is the deviations.

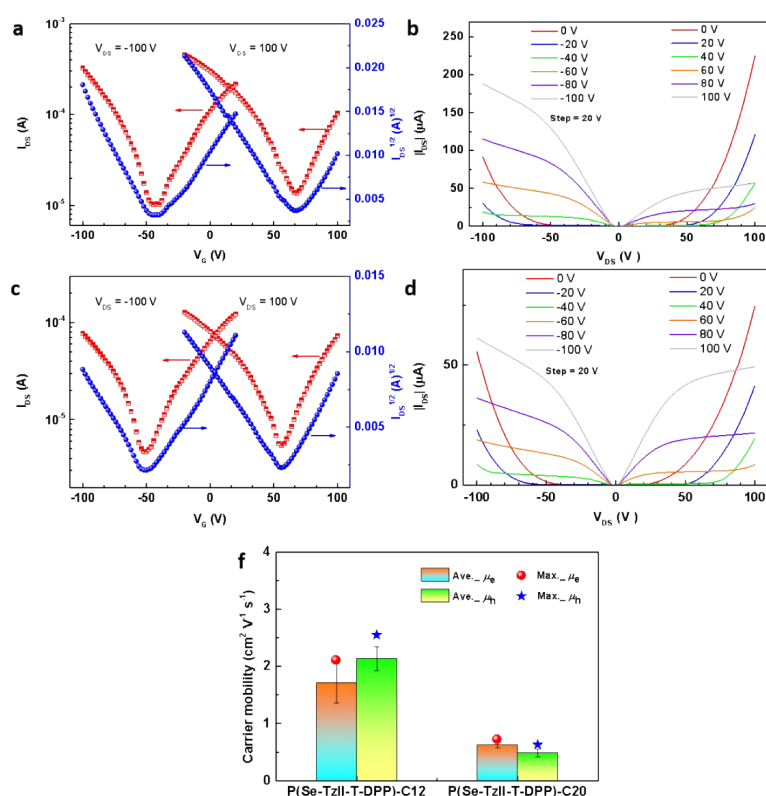


Figure S12. (a, c) transfer curves and (b, d) output characteristics of OFET devices based on the polymers P(Se-TzII-T-DPP)-C12 and P(Se-TzII-T-DPP)-C20 films annealed at $280\ \text{°C}$. (e) The electron and hole mobility distribution profile.

8. X-ray diffraction and morphology Study

The X-ray diffraction data were obtained at beamline BL14B1 of the Shanghai Synchrotron Radiation Facility (SSRF) at a wavelength of 1.2398 Å. BL14B1 is a beamline based on bending magnet and a Si (111) double crystal monochromator was employed to monochromatize the beam. The size of the focus spot is about 0.5 mm and the end station is equipped with a Huber 5021 diffractometer. NaI scintillation detector was used for data collection. Atomic force microscopy studies were performed with a Nanoscope IIIa microscope (Extended Multimode). All experiments were carried out in tapping mode under ambient conditions. A silicon nitride cantilever (Budget Sensors Tap300A1) was used with a resonant frequency around 300 kHz.

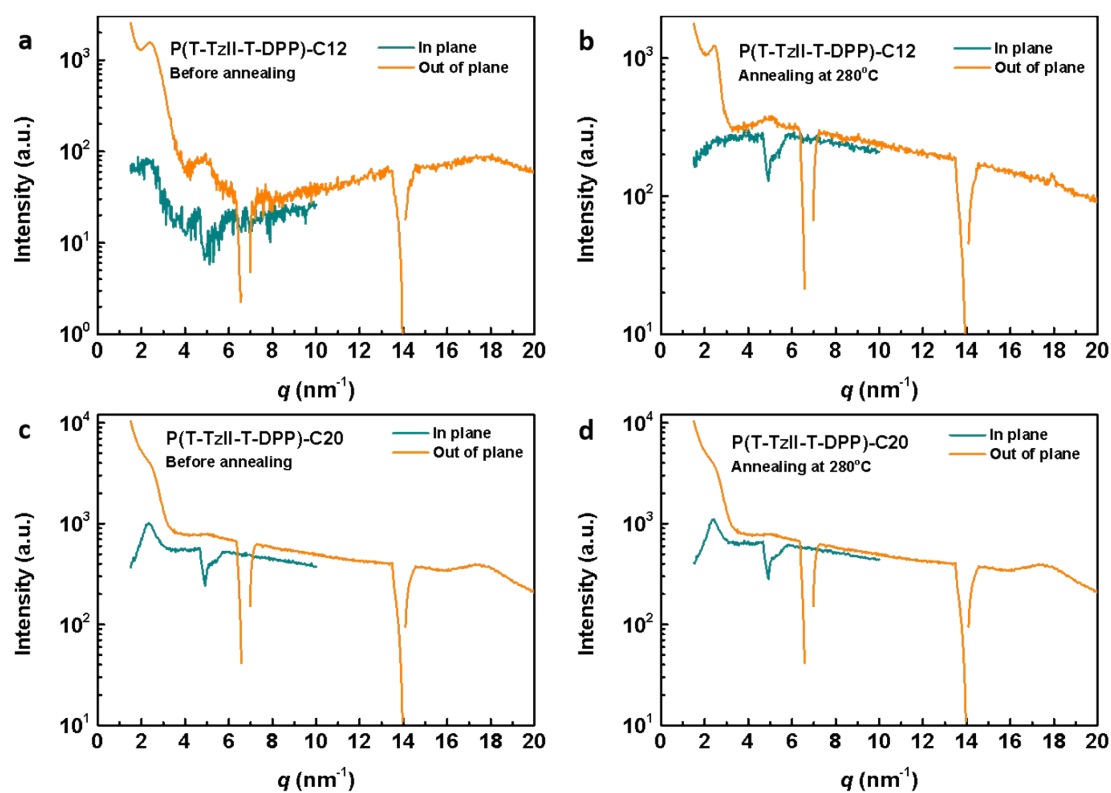


Figure S13. In and out-of-plane GIWAXS before and after annealing at 280 °C for polymers (a, b) P(T-TzII-T-DPP)-C12 and (c, d) P(T-TzII-T-DPP)-C20, respectively.

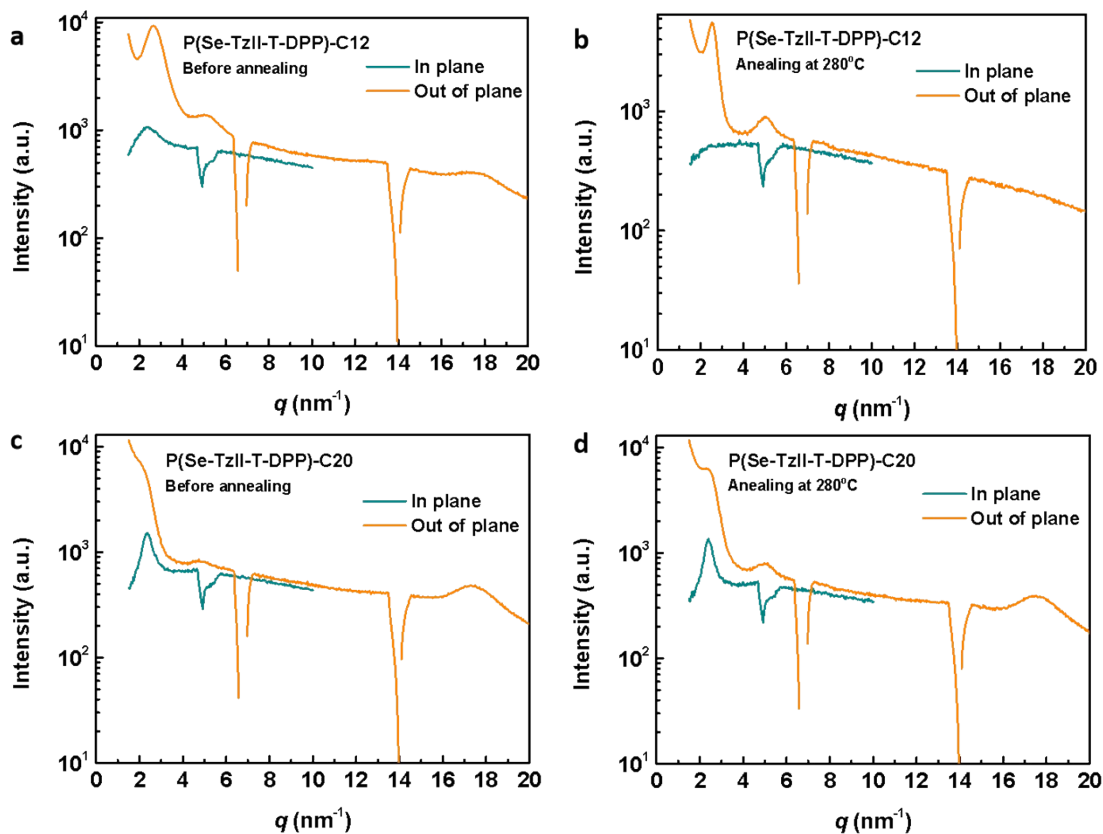


Figure S14. In and out of-plane GIWAXS before and after annealing at 280 °C for polymers (a, b) P(Se-TzII-T-DPP)-C12 and (c, d) P(Se-TzII-T-DPP)-C20, respectively.

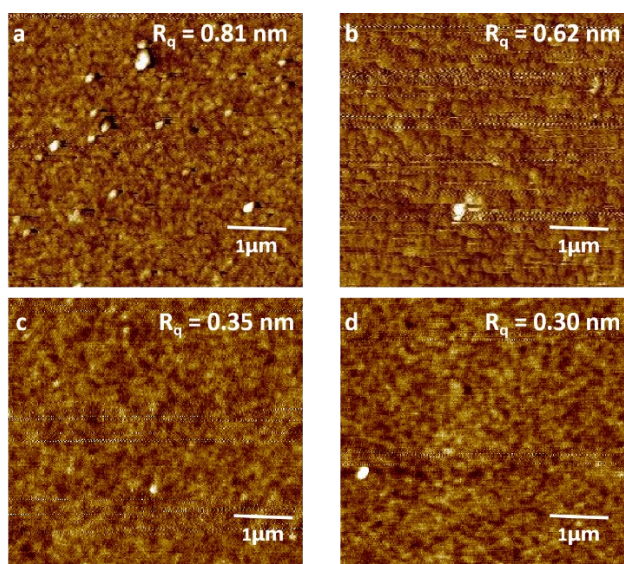
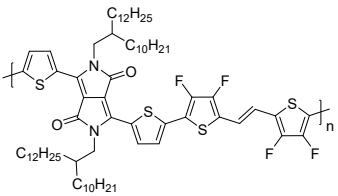
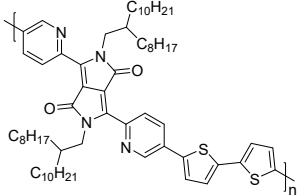
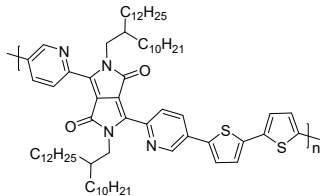
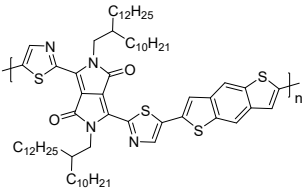
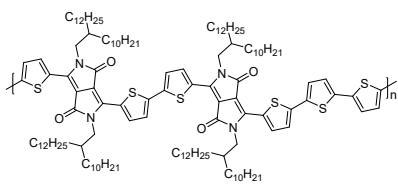
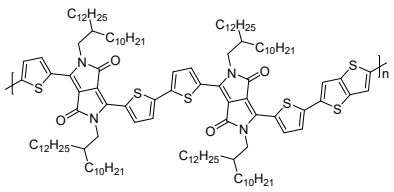
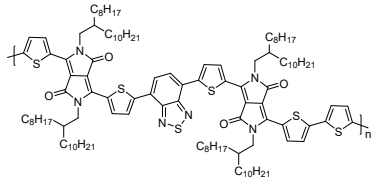
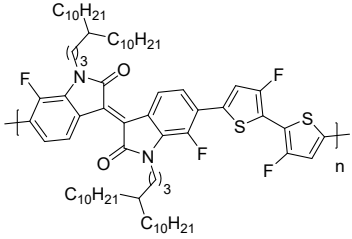
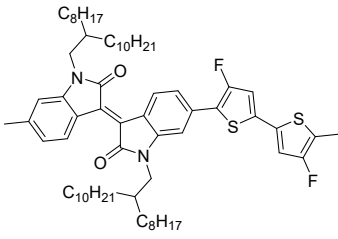
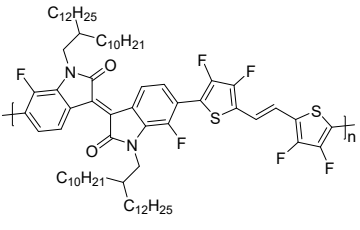
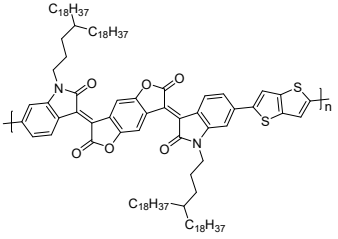
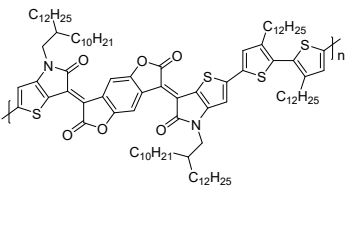
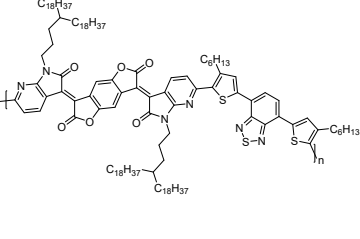


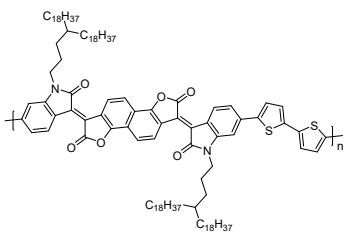
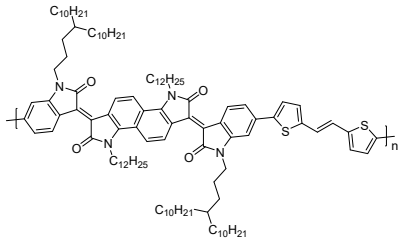
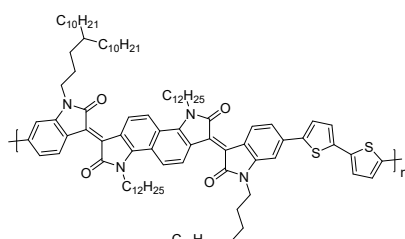
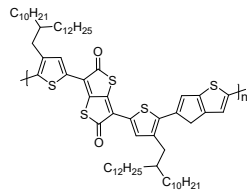
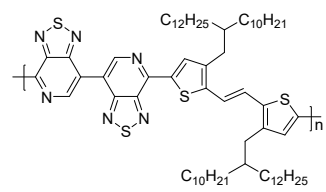
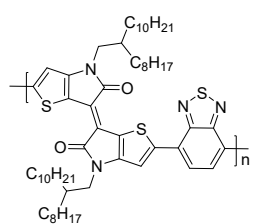
Figure S15. $5 \times 5 \mu\text{m}^2$ tripping-mode AFM height images of (a) P(T-TzII-T-DPP)-C12, P(T-TzII-T-DPP)-C20, P(Se-TzII-T-DPP)-C12, and P(Se-TzII-T-DPP)-C20 before annealing.

Table S5. The representative ambipolar polymers for OFET.

Dipyrrolopyrrolidone (DPP) -based ambipolar polymers	Polymers			
	Maximum μ_e ($\text{cm}^2 \text{V}^{-1} \text{s}^{-1}$)	5.86	6.30	1.05
	Maximum μ_h ($\text{cm}^2 \text{V}^{-1} \text{s}^{-1}$)	3.40	2.78	0.86
	μ_e/μ_h	1.72	2.27	1.22
	Ref.	[S3]	[S4]	[S5]
	Polymers			
Maximum μ_e ($\text{cm}^2 \text{V}^{-1} \text{s}^{-1}$)	5.33	2.60	3.01	
Maximum μ_h	5.47	2.99	4.16	

	$(\text{cm}^2 \text{V}^{-1} \text{s}^{-1})$			
	μ_e/μ_h	0.97	0.87	0.72
	Ref.	[S6]	[S7]	[S7]
Polymers				
	Maximum μ_e ($\text{cm}^2 \text{V}^{-1} \text{s}^{-1}$)	7.71		
	Maximum μ_h ($\text{cm}^2 \text{V}^{-1} \text{s}^{-1}$)	8.90		
	μ_e/μ_h	0.87		
	Ref.	[S8]		
Isoindigo (IID) - based ambipolar polymers				
	Maximum μ_e	6.76	0.09	3.50

	(cm ² V ⁻¹ s ⁻¹)			
	<i>Maximum</i> μ_h (cm ² V ⁻¹ s ⁻¹)	6.41	0.09	3.94
	μ_e/μ_h	1.05	1	0.89
	Ref.	[S9]	[S10]	[S11]
BDOPV-based ambipolar polymers	Polymers			
	<i>Maximum</i> μ_e (cm ² V ⁻¹ s ⁻¹)	1.70	0.22	7.07
	<i>Maximum</i> μ_h (cm ² V ⁻¹ s ⁻¹)	1.27	0.45	5.97
	μ_e/μ_h	1.34	0.49	1.18
	Ref.	[S12]	[S13]	[S14]

NBDOPV-based ambipolar polymers	Polymers			
	<i>Maximum</i> μ_e ($\text{cm}^2 \text{V}^{-1} \text{s}^{-1}$)	0.50	0.16	0.61
	<i>Maximum</i> μ_h ($\text{cm}^2 \text{V}^{-1} \text{s}^{-1}$)	0.51	0.45	1.66
	μ_e/μ_h	0.98	0.36	0.37
	Ref.	[S15]	[S16]	[S17]
Other ambipolar polymers	Polymers			
	<i>Maximum</i> μ_e ($\text{cm}^2 \text{V}^{-1} \text{s}^{-1}$)	0.14	8.49	0.14

	<i>Maximum</i> μ_h (cm ² V ⁻¹ s ⁻¹)	0.14	6.87	0.14
	μ_e/μ_h	1	1.24	1
	Ref.	[S18]	[S19]	[S20]

Reference

- [S1] Cui Y, Zhu P, Shi X, et al. Theoretical Study of Excited State Charge Transfer Characteristics based on A–D–A and A–DA' D–A Type Nonfullerene Acceptors[J]. *The Journal of Physical Chemistry C*, 2021, 125(19): 10250-10259.
- [S2] Lu T, Chen F. Multiwfn: a Multifunctional Wavefunction Analyzer[J]. *Journal of computational chemistry*, 2012, 33(5): 580-592.
- [S3] Gao Y, Zhang X, Tian H, et al. High Mobility Ambipolar Diketopyrrolopyrrole-Based Conjugated Polymer Synthesized via Direct Arylation Polycondensation[J]. *Advanced Materials*, 2015, 27(42): 6753-6759.
- [S4] Sun B, Hong W, Yan Z, et al. Record high electron mobility of $6.3 \text{ cm}^2\text{V}^{-1} \text{ s}^{-1}$ achieved for polymer semiconductors using a new building block[J]. *Advanced Materials*, 2014, 26(17): 2636-2642.
- [S5] Guo K, Bai J, Jiang Y, et al. Diketopyrrolopyrrole-Based Conjugated Polymers Synthesized via Direct Arylation Polycondensation for High Mobility Pure n-Channel Organic Field-Effect Transistors[J]. *Advanced Functional Materials*, 2018, 28(31): 1801097.
- [S6] Xiao C, Zhao G, Zhang A, et al. High-performance Polymer Nanowire Field-Effect Transistors with Distinct Molecular Orientations[J]. *Advanced Materials*, 2015, 27(34): 4963-4968.
- [S7] Yang J, Wang H, Chen J, et al. Bis-diketopyrrolopyrrole Moiety as a Promising Building Block to Enable Balanced Ambipolar Polymers for Flexible Transistors[J]. *Advanced Materials*, 2017, 29(22): 1606162.
- [S8] Ni Z, Wang H, Zhao Q, et al. Ambipolar Conjugated Polymers with Ultrahigh Balanced Hole and Electron Mobility for Printed Organic Complementary Logic via a Two-Step C-H Activation Strategy[J]. *Advanced materials*, 2019, 31(10): 1806010.
- [S9] Yang J, Zhao Z, Geng H, et al. Isoindigo-Based Polymers with Small Effective Masses for High-Mobility Ambipolar Field-Effect Transistors[J]. *Advanced Materials*, 2017, 29(36): 1702115.
- [S10] Kim M, Park W T, Park S A, et al. Controlling Ambipolar Charge Transport in Isoindigo-Based Conjugated Polymers by Altering Fluorine Substitution Position for

High-Performance Organic Field-Effect Transistors[J]. *Advanced Functional Materials*, 2019, 29(10): 1805994.

[S11] Gao Y, Deng Y, Tian H, et al. Multifluorination toward High-mobility Ambipolar and Unipolar n-type donor-acceptor Conjugated Polymers based on Isoindigo[J]. *Advanced Materials*, 2017, 29(13): 1606217.

[S12] Zhou X, Ai N, Guo Z H, et al. Balanced Ambipolar Organic Thin-film Transistors Operated under Ambient Conditions: Role of the Donor Moiety in BDOPV-based Conjugated Copolymers[J]. *Chemistry of Materials*, 2015, 27(5): 1815-1820.

[S13] Zhang G, Ye Z, Li P, et al. A new Thieno-isoindigo Derivative-based D-A Polymer with Very Low Bandgap for High-performance Ambipolar Organic Thin-film Transistors[J]. *Polymer Chemistry*, 2015, 6(21): 3970-3978.

[S14] Shi K, Zhang W, Gao D, et al. Well-Balanced Ambipolar Conjugated Polymers Featuring Mild Glass Transition Temperatures Toward High-Performance Flexible Field-Effect Transistors[J]. *Advanced Materials*, 2018, 30(9): 1705286.

[15] Deng Y, Sun B, He Y, et al. (3 E, 8 E)-3, 8-Bis (2-oxoindolin-3-ylidene) naphtho-[1, 2-b: 5, 6-b'] difuran-2, 7 (3 H, 8 H)-dione (INDF) based Polymers for Organic Thin-film Transistors with Highly Balanced Mmbipolar Charge Transport Characteristics[J]. *Chemical Communications*, 2015, 51(70): 13515-13518.

[16] Jiang Y, Gao Y, Tian H, et al. Synthesis and Characterization of Isoindigo [7, 6-g] Isoindigo-based Donor-acceptor Conjugated Polymers[J]. *Macromolecules*, 2016, 49(6): 2135-2144.

[17] Huang K, Zhao X, Du Y, et al. Modulating Charge Transport Characteristics of Bis-azaisoindigo-based D-A conjugated Polymers Through Energy Level Regulation and Side Chain Optimization[J]. *Journal of Materials Chemistry C*, 2019, 7(25): 7618-7626.

[18] Kawabata K, Osaka I, Nakano M, et al. Thienothiophene-2, 5-Dione-Based Donor-Acceptor Polymers: Improved Synthesis and Influence of the Donor Units on Ambipolar Charge Transport Properties[J]. *Advanced Electronic Materials*, 2015, 1(6): 1500039.

[19] Zhu C, Zhao Z, Chen H, et al. Regioregular Bis-pyridal [2, 1, 3] Thiadiazole-based

Semiconducting Polymer for High-performance Ambipolar Transistors[J]. Journal of the American Chemical Society, 2017, 139(49): 17735-17738.

[20] Ashraf R S, Kronemeijer A J, James D I, et al. A New Thiophene Substituted Isoindigo based Copolymer for High Performance Ambipolar Transistors[J]. Chemical communications, 2012, 48(33): 3939-3941.